Surface Modifications of Nano-Structured Cathodes to Enhance Durability of Intermediate Temperature Solid Oxide Fuel Cells

ECS Transactions, 91 (1) 1263-1272 (2019)
10.1149/09101.1263ecst ©The Electrochemical Society

Surface Modifications of Nano-structured Cathodes to Enhance Durability of Intermediate Temperature Solid Oxide Fuel Cells

Yeting Wen[a], Tianrang Yang[a], Dongkyu Lee[a, b], Ho Nyung Lee[b], Ethan J. Crumlin[c] and Kevin Huang [a*]

[a] Department of Mechanical Engineering, University of South Carolina, Columbia, South Carolina 29201, USA
[b] Materials Sciences and Technology Division, Oak Ridge National Laboratory, Oak Ridge, Tennessee 37831, USA
[c] Advanced Light Source, Lawrence Berkeley National Laboratory, Berkeley, California 94720, USA
*Corresponding author: huang46@cec.sc.edu

The bulk-to-surface Sr-segregation can seriously compromise the stability of oxygen electrocatalysis in Sr-doped perovskite oxides such as $La_{1-x}Sr_xCoO_{3-\delta}$ and $La_{1-x}Sr_xCo_{1-y}Fe_yO_{3-\delta}$ and limit their practical applications as cathode materials in solid oxide fuel cells. This work aims to acquire fundamental knowledge of Sr-segregation process under practical conditions in solid oxide fuel cells and develop suppression method to ensure the long-term stability through surface modifications. In this work, the pristine and ZrO_2 atomic layer deposition (ALD) modified $La_{0.6}Sr_{0.4}CoO_{3-\delta}$ (LSCo) epitaxial films were used as the model systems to investigate how the temperature, time and surface coating affect the surface concentration of Sr via *in situ* synchrotron-based ambient pressure XPS. This information was also correlated with their electrochemical performances characterized by electrochemical impedance spectroscopy. We also report a Sr-segregation-free $SrCo_{0.9}Ta_{0.1}O_{3-\delta}$ (SCT) multifunctional coating on a benchmark cathode LSCF as a means of enhancing ORR activity and durability against Cr-poison.

Introduction

The Sr-doped perovskites are very promising cathode materials for solid oxide fuel cells (SOFCs) due to high mixed electronic/oxide-ionic conductivity and high oxygen reduction reaction (ORR) activity. One critical issue with these Sr-doped perovskites such as $La_{0.6}Sr_{0.4}Co_{0.2}Fe_{0.8}O_{3-\delta}$ (LSCF) and $La_{0.6}Sr_{0.4}CoO_{3-\delta}$ (LSCo) is the Sr-segregation originated from the electrostatic interaction between dopant ( ) and oxygen vacancy ( ) (1, 2). The main compositions of the segregated Sr-rich phase identified so far are insulating SrO, $SrCO_3$ and/or $Sr(OH)_2$ (3-5), a coverage of which rapidly diminishes the original high ORR activity stemming from the strong O-2p and Co-3d orbital covalent mixing, causing performance decay (6-9). Moreover, the segregated SrO can react with H_2O and CO_2 in ambient air and the Cr species from interconnects to form more Sr-contained insulators (5, 10-12). Thus, it is necessary to acquire the fundamental knowledge of Sr-segregation as well as the suppression method.

The aim of the present study is to investigate how the temperature, time and surface coating affect the surface concentration of Sr in a $La_{1-x}Sr_xCoO_{3-\delta}$ epitaxial film by using *in situ* synchrotron-based ambient pressure XPS (APXPS) (13), a cutting-edge surface analysis technique. To precisely control the thickness and chemistry of the surface coating, atomic layer deposition (ALD) is applied to make a nanoscaled ZrO_2 layer over the $La_{1-x}Sr_xCoO_{3-\delta}$ epitaxial films. On the other hand, a continuous $SrCo_{0.9}Ta_{0.1}O_{3-\delta}$ (SCT10) nanoscaled capping layer which is Sr-segregation-free and highly active was used to overcoat a pre-fabricated porous LSCF-GDC skeleton (SCT@LSCF-GDC) to improve its ORR activity and the resistance against Cr-poison.

Experimental

The 50 nm thick epitaxial $La_{0.6}Sr_{0.4}CoO_3$ (LSCo) thin films were grown on (001)-oriented YSZ by pulsed laser deposition (PLD). Single crystal 9.5 mol% YSZ wafers with the (001) cubic orientation and dimensions of 10 × 5 × 0.5 mm (MTI corporation, USA) were used as the substrate. The 5 nm thick Gd-doped CeO_2 (GDC) buffer layer was also deposited by PLD between YSZ single crystal and LSCo epitaxial film to prevent the formation of $La_2Zr_2O_7$ (14) at the interface (15). PLD was performed using a KrF excimer laser at λ = 248 nm, 10 Hz pulse rate, and 50 mJ pulse energy under a pO_2 of 6.6×10^{-5} atm (50 mTorr). A total of 500 pulses were applied to YSZ single crystal substrate at 550 °C for GDC film, and a total of 5,000 pulses were applied to GDC/YSZ-substrate at 650 °C for LSCo film. A precise 0.8 nm thick ZrO_2 layer was further coated on top of the LSCo epitaxial film by ALD in a flow-type reactor (Ultratech Savannah 200 series). Tetrakis (dimethylamido) zirconium (IV) (electronic grade, ≥ 99.99%, Sigma-Aldrich) and deionized (DI) water were used as Zr-precursor and oxidant, respectively. The reactor temperature was controlled at 180 °C. The pre-determined deposition rate is 0.1nm/cycle for ALD-ZrO_2, which requires 8 cycles to yield a 0.8 nm thick layer of ZrO_2.

The bi-layer structured SCT@LSCF-GDC cell was first fabricated by screen printing an LSCF-GDC ($La_{0.6}Sr_{0.4}Co_{0.2}Fe_{0.8}O_{3-\delta}$–$Gd_{0.1}Ce_{0.9}O_{1.95}$) ink (purchased from Fuelcellmaterials, 50:50 of weight ratio) on both sides of a 300 μm thick $Gd_{0.1}Ce_{0.9}O_{2-\delta}$ (GDC10, Fuelcellmaterials) dense pellet, followed by firing at 1100 °C for 2 h to form the LSCF-GDC skeleton with the thickness of ~25 μm. The infiltration solution was made by the following procedures: citric acid (Sigma-Aldrich) was first dissolved in a de-ionized water, then mixed with a stoichiometric amount of $Sr(NO_3)_2$ (Alfa Aesar) and $Co(NO_3)_2{\cdot}6H_2O$ (Alfa Aesar). A separate solution containing ethylene diamine tetraacetic acid (EDTA, Sigma-Aldrich) and diluted ammonia water was then added into the above solution and adjust the pH to 8. A stoichiometric amount of $Ta(OC_2H_5)_5$ (Sigma-Aldrich) was dissolved into pure ethanol and then slowly added into the above solution to achieve the solution for infiltration. The total metal-ions concentration was 0.2 M. Citric acid, EDTA and metal ions have the molar ratio of 2:1:1. Water and ethanol have a volume ratio of 5:1 in the final solution. Then the SCT solution was dropped into the LSCF-GDC skeleton and followed by thermal treatment at 500 °C for 1 h. The infiltration process was repeated for about 10 times to reach 20% SCT loading (based on the weight of LSCF) and followed by the calcination at 1000 °C for 2 h.

Oxide phase purity and orientation of the deposited thin films were investigated via high resolution X-ray diffraction (HRXRD) using a four-circle diffractometer. The *in-situ* APXPS spectra were collected at Beamline 9.3.2 of Advanced Light Source at Lawrence

Berkeley National Laboratory (16). The sample was first placed on a heater on which a thermocouple was attached to measure the temperature. A pair of the pristine and overcoated thin film samples was used to investigate the surface equilibrium concentration of Sr from 25 to 520 °C. The heating rate was controlled at 3~5 °C per minute with a holding period of 3 h at 200, 350, 450 and 520 °C under a constant oxygen partial pressure of 1×10^{-3} atm. The spectra collection started with two survey scans (BE = 10 – 590 eV) at a photon energy of 690 and 695 eV to remove the Auger peaks and continued with the Sr 3d and La 4d spectra in every 12 min during the whole heating process. Scanning transmission electron microscope (STEM, Hitachi HD-2000) imaging equipped with energy-disperse x-ray spectroscopy (EDX) were employed to obtain images as well as analyze chemical compositions of bi-layer structured SCT@LSCF-GDC cells. The EIS spectra of thin film and symmetrical cells were collected with a Solartron 1470/1455B multi-channel electrochemical station in a frequency range of 0.01 Hz - 1 MHz and AC amplitude of 10 mV.

Results and discussion

Epitaxial $La_{0.6}Sr_{0.4}CoO_3$ (LSCo) thin films(17)

The HRXRD θ-2θ patterns collected at RT are shown in Figure 1a, where only (00l) (l is integer) peaks of LSCo, GDC, and YSZ can be seen, implying that the LSCo films were highly oriented with the (001) orientation of the single-crystal YSZ substrate. The 0.8 nm thick ZrO_2 overcoat did not bring discernible change in the XRD pattern of LSCo. Off-normal ϕ scan analysis of the multilayer with and without ZrO_2 overcoat shown in Figure 1b reveals only {202} plane family for LSCo, GDC and YSZ layers, suggesting a 4-fold cubic symmetry and a cube-on-cube alignment of GDC on YSZ and 45º in-plane rotation of LSCo on GDC. The relaxed lattice parameters of both epitaxial LSCo films obtained in this study are in a close range of 3.828 – 3.831 Å, indicating the very thin ZrO_2 layer has no influence on in-plane and out-of-plane strains of the LSCo thin film underneath. Therefore, we can ignore the strain effect of ZrO_2 overcoat on the LSCo film.

The Sr 3d and La 4d spectra of the pristine and ALD-coated LSCo films were collected in every 12 min within a temperature range of 25 to 520 °C at a fixed oxygen partial pressure of 1×10^{-3} atm. The Sr 3d spectra were used to analysis the Sr components and determine the time needed to reach equilibrium concentration at each selected temperature. The La 4d spectra were used to calibrate the peak positions due to the unstable beam energy, and thus the binding energies of same element sometimes are slightly different between pristine and coated sample and different temperatures. In general, the Sr 3d peaks can be divided into 2 sets of Sr $3d_{5/2}$ and $3d_{3/2}$ doublets that belong to surface and lattice Sr (18). The lower-energy set of Sr 3d is assigned to lattice Sr, whereas the higher set can be assigned to surface Sr which could contains SrO and $Sr(OH)_2$, respectively.. The presence of $SrCO_3$ phase can be ruled out because of the lack of C 1s peak when the temperature was above 250 °C. The time-dependent Sr 3d spectra of both samples under 350 °C are shown in Figure 2a and 2b as an example. The shape of the spectra remains almost the same from 0 to 0.6 h after the temperature was increased to 350 °C. The obtained peak area ratios of the surface Sr are further shown as a function of time in Figure 2c for pristine and coated samples, respectively. It is obvious that the surface Sr ratio of both samples were increasing with the temperature and stabilized as soon as the temperature reached the set point, implying that the surface Sr-segregation

process is rather quick. Furthermore, its fast stabilization with temperature is also supported by the theory that the Sr-segregation is mainly governed by chemical diffusion which is greatly affected by temperature (19). As a result, the Sr segregation stops when it meets the thermal equilibrium and proceeds again after increasing in temperature. At 520 °C, the area ratio of surface Sr components is similar for both samples, but the actual amount of surface Sr components should be presented by quantification analysis.

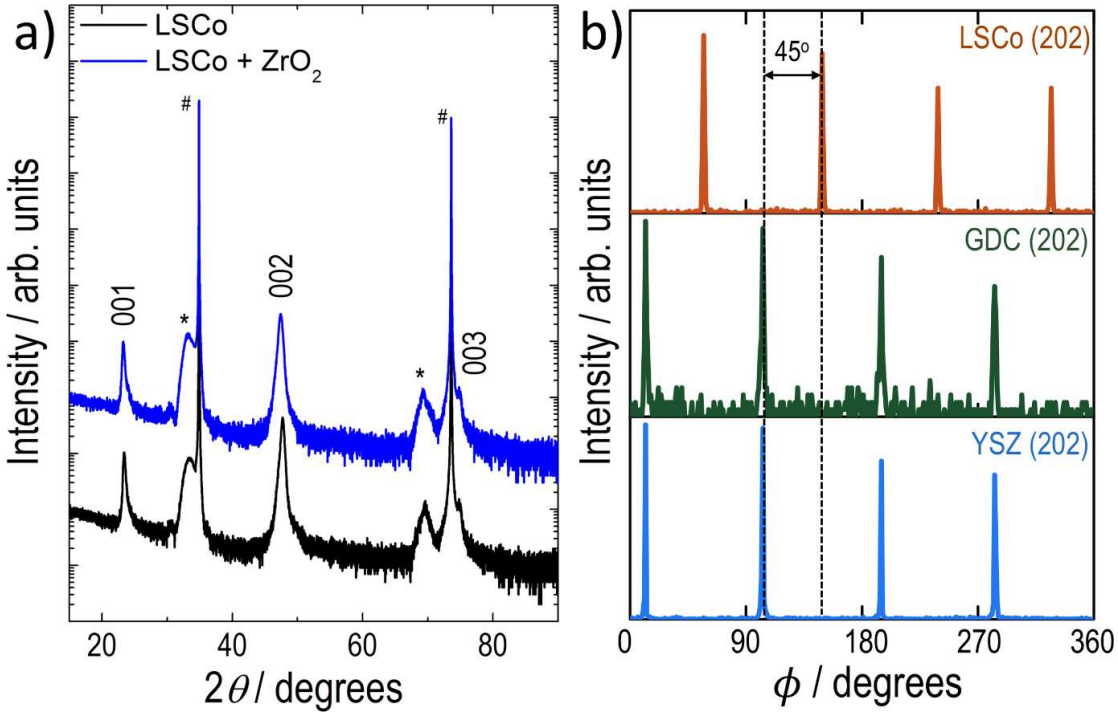

Figure 1. High resolution X-ray diffraction analysis at RT. (a) Normal XRD of the epitaxial LSCo thin film (black) and LSCo film coated with ZrO_2 (blue). GDC and YSZ substrate peaks are indicated with ∗ and #, respectively. (b) Off-normal XRD of the (202) reflection of a YSZ substrate (light blue), a GDC buffer layer (green), and the (202) reflection of a LSCo thin film (red), confirming the cube-on-cube alignment of GDC on YSZ and 45° in-plane rotation of LSCo on GDC.

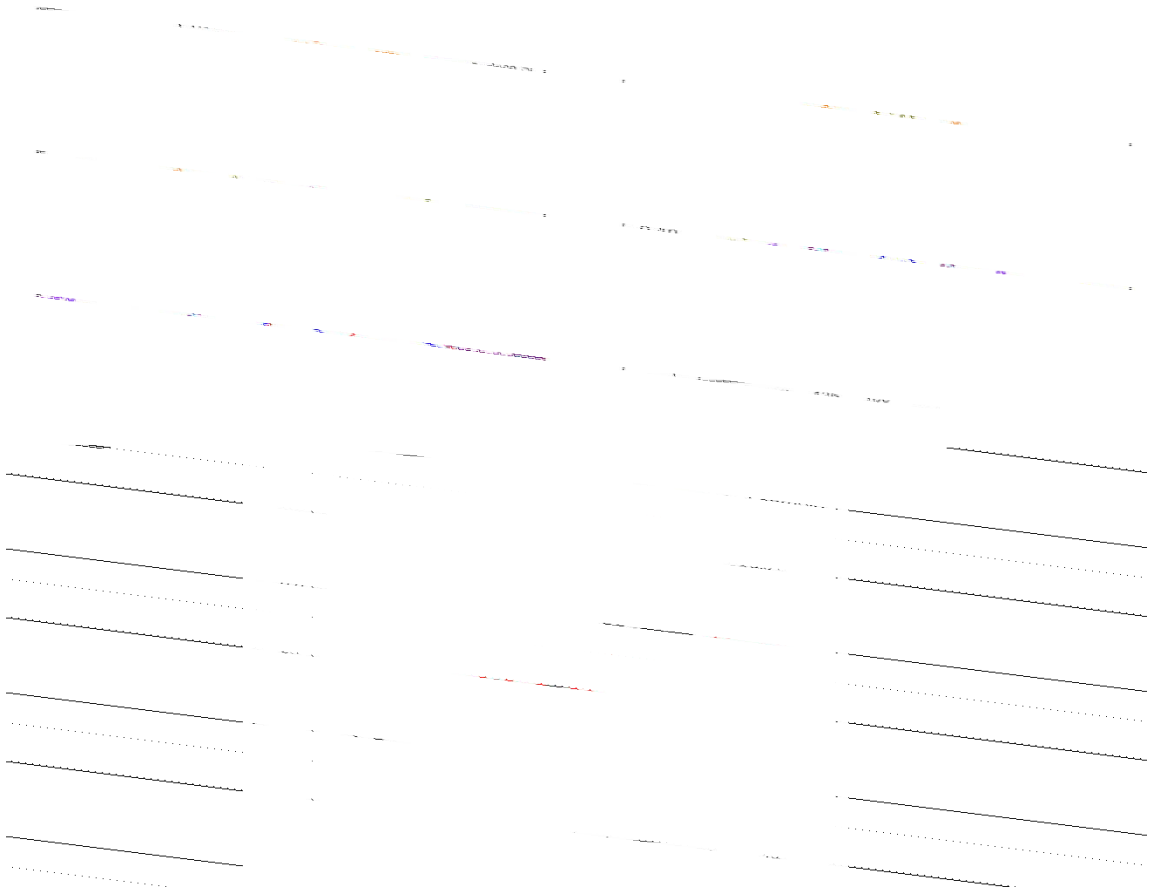

Figure 2. Time-dependent Sr 3d spectra for a) pristine and b) coated sample at 350 °C; time-dependent area ratio of surface Sr for pristine and coated sample during the heating process from 200 to 520 °C in an oxygen pressure of 1×10^{-3} atm.

Due to the existence of ZrO_2 layer on the surface of the coated sample, the surface Sr-ratio cannot fairly represent the actual amount of surface Sr-segregation in both the pristine and coated samples. So, the atomic fraction of La, Sr, Co, O and Zr (denoted as [La], $[Sr]_{tot}$, [Co], [O] and [Zr], respectively) were calculated based on their normalized intensities that were obtained by normalizing the peak area with photoionized cross-section and inelastic mean free path of each elements; this is a technique that has previously been used elsewhere (18, 20). The results from 250 to 520 °C (RT data was not included due to the adsorbed surface contaminations) are shown in Figure 3a and 3b, where the atomic fraction of each element is compared for the two samples. For the pristine sample at RT, $[Sr]_{tot}$ is larger than [La] and [Co] because of the existence of rich surface Sr components. From 250 to 520 °C, $[Sr]_{tot}$ is increased gradually because of the Sr-segregation from the bulk towards the near surface region where XPS can detect. For the coated sample, [Zr] and [O] are dominant over the entire temperature range studied because XPS is only sensitive to the near surface region and the thickness of ZrO_2 is close to the probe depth. From a direct comparison, the $[Sr]_{tot}$ for coated sample is greatly smaller than that of pristine sample, implying the effective Sr-segregation suppression by ZrO_2 thin layer.

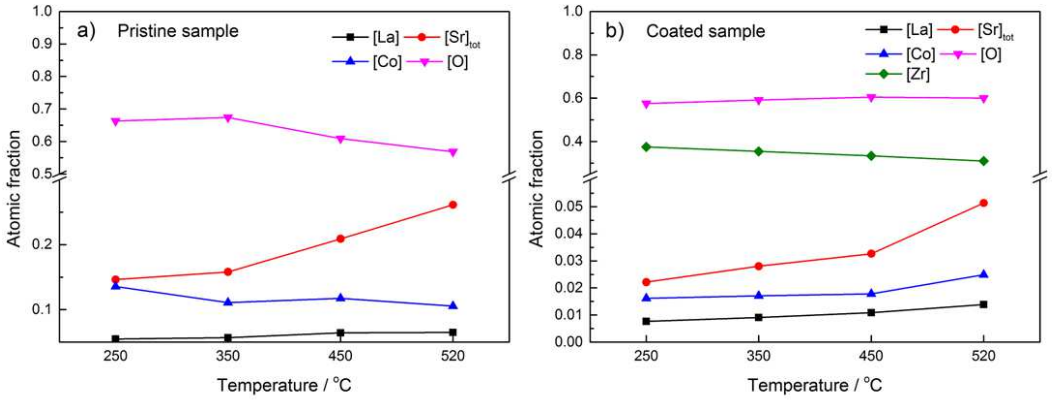

Figure 3. Temperature-dependent atomic concentrations of a) pristine and b) ALD-coated sample.

The time-dependent EIS measurements were performed to characterize the stability of electrochemical performance of the pristine and coated LSCo films. The EIS spectra and the obtained R_p values during 300 h for the two samples are compared in Figure 4a and 4b, respectively. From the beginning, R_p of the pristine sample was larger than that of the coated one due to the Sr-segregation. As the time elapses, R_p of the pristine sample grows precipitously with time at a rate of 4.3 ohm·cm^2/h, while for the coated sample, the R_p increases at a much smaller rate of 0.9 ohm·cm^2/h, further demonstrating of beneficial effect of ALD-ZrO_2 coating in stabilizing the polarization resistance. The low-frequency $R_{p(LF)}$ is associated with the oxygen adsorption/dissociation process, *i.e.* surface oxygen exchange process (21, 22), and can be used to calculate the surface exchange coefficient k^q (23) as shown in Figure 4c. The k^q of the coated sample is in reasonable range of the reported value (24, 25), and about 2× higher than that of pristine sample at the beginning of the test and 4× higher at 300-h marker. For the thin film sample, there is no structural complexity, meaning that such difference should not be attributed to geometrical effects, but to the true chemical state in the near-surface region. Therefore, a much stable R_p of the coated samples is another strong evidence of the suppressed Sr segregation by the ZrO_2 layer, consistent with the APXPS results.

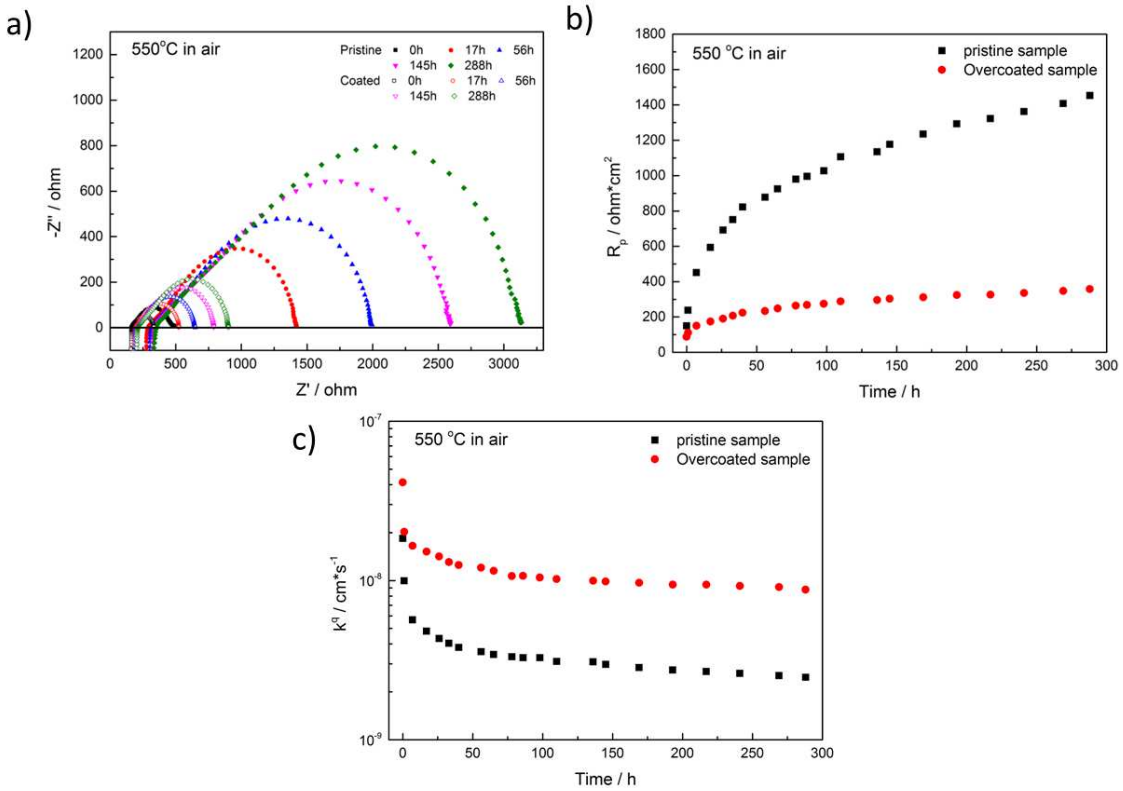

Figure 4. a) Comparison of Nyquist plots of pristine and coated sampled for select time intervals; b) time-dependent R_p values and c) surface oxygen exchange coefficients vs time of the pristine and coated samples measured at 550 ^oC in air.

Bi-layer structured SCT@LSCF-GDC (26)

The STEM image of SCT10@LSCF-GDC cell is shown in Figure 5 which clearly reveals a continuous, intimately bonded bilayer structure. The compositional analysis by STEM-EDX indicates that Ta from SCT mostly concentrates in the outer layer, suggesting that SCT serves as the overcoat around LSCF-GDC particles via the 1000 °C-calcination infiltration. Figure 6 shows the extracted R_P *vs* time at 700 °C for both the pristine and bilayer electrode. At the beginning of the test in clean air, the bilayer electrode clearly outperforms the pristine one by demonstrating at least 3× lower R_P, and both electrodes show reasonable stability. After the cells are exposed to Cr-contained alloy, the R_p of LSCF-GDC experienced a significant increase from 0.51 to 1.35 Ωcm^2. The increase is very high at the beginning and followed with a lower increase which is in agreement with the other study (27). The effect of Cr is quite different for SCT@LSCF-GDC: there is only a slight increase of R_p when Cr was added and the total performance degradation after 1000 h test is only 0.1 Ωcm^2.

The significant difference in electrochemical performance degradation and Cr deposition for LSCF-GDC and SCT@LSCF-GDC reveals the excellent durability against Cr-poison introduced by SCT coating. A lot of efforts have been given to understand the Cr-poison mechanisms. It is commonly believed that the formation of Cr-containing secondary phase such as $SrCrO_4$ serves as an insulator covering the cathode surface (28-31). Also, it has been found out that the segregated Sr from the LSCF bulk can greatly

enhance the deposition of Cr species (32). SrO was identified to be the nucleation agent for Cr deposition (11, 12). As a conformal layer, the SCT coating can separate LSCF from gaseous Cr species, and there is no SrO on the surface of SCT to initiate Cr deposition due to its Sr-segregation-free feature. The excellent resistance of SCT coating against Cr-poison has a profound meaning for the practical application of SCT@LSCF-GDC composite as cathode of SOFC.

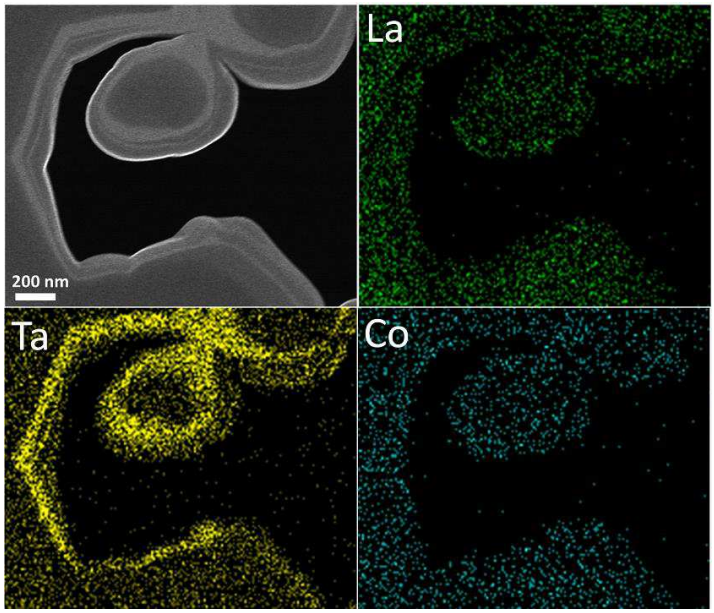

Figure 5. The STEM image and EDX mapping of SCT10@LSCF-GDC bilayer structured cell.

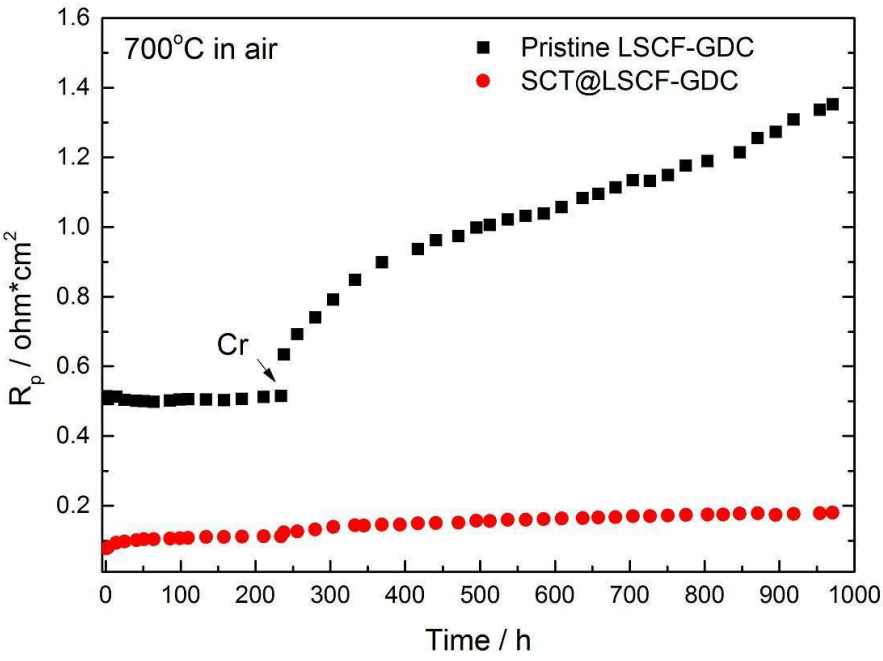

Figure 6. Time-dependent R_p values for LSCF-GDC and SCT@LSCF-GDC electrodes unexposed and exposed to Cr-contained alloy at 700 °C in air for 1000 h.

Conclusions

The Sr bulk-to-surface segregation of pristine and ALD-ZrO_2-overcoated LSCo epitaxial films investigated by *in-situ* APXPS as a function of time and temperature at a fixed oxygen partial pressure of 1×10^{-3} atm show fast kinetics, but the amount of surface Sr in the coated sample is significantly lower than that of the pristine sample. EIS study reveals that the coated sample exhibits a more stable ORR activity than the pristine sample at 550 °C in ambient air over 300 h. Overall, it is concluded that the ALD-ZrO_2 thin layer is effective in suppressing bulk-to-surface Sr segregation in oxygen-vacancy-rich Sr-doped perovskites. The SCT coating has greatly improved the ORR activity and the long-term stability of LSCF-GDC. In addition, the SCT coating also shows great resistance against Cr-poison due to its Sr-segregation-free feature. The initial polarization resistance of SCT@LSCF-GDC at 700 °C is only 20% of pristine LSCF-GDC and the performance degradation is only 0.1 *vs* 0.84 Ωcm^2 under Cr-poison.

Acknowledgments

This work was funded by the Advanced Research Projects Agency-Energy (ARPA-E), U.S. Department of Energy, under award number DE-AR0000492 and Office of Fossil Energy, U.S. Department of Energy, under award number DE-FE-0023317, and National Science Foundation, under award number of DMR-1464112.

References

1. W. Jung and H. L. Tuller, *Energy & Environmental Science*, **5**, 5370 (2012).
2. W. Lee, J. W. Han, Y. Chen, Z. Cai and B. Yildiz, *J Am Chem Soc*, **135**, 7909 (2013).
3. S. Jiang and J. Love, *Solid State Ion.*, **138**, 183 (2001).
4. P. Hjalmarsson, M. Søgaard and M. Mogensen, *Solid State Ion.*, **179**, 1422 (2008).
5. Y. Yu, H. Luo, D. Cetin, X. Lin, K. Ludwig, U. Pal, S. Gopalan and S. Basu, *Appl. Surf. Sci.*, **323**, 71 (2014).
6. M. Kubicek, A. Limbeck, T. Frömling, H. Hutter and J. Fleig, *J. Electrochem. Soc.*, **158**, B727 (2011).
7. R. Bertacco, J. Contour, A. Barthélemy and J. Olivier, *Surf. Sci.*, **511**, 366 (2002).
8. Y. Chen, W. Jung, Z. Cai, J. J. Kim, H. L. Tuller and B. Yildiz, *Energy Environ. Sci.*, **5**, 7979 (2012).
9. M. Finsterbusch, A. Lussier, J. Schaefer and Y. Idzerda, *Solid State Ion.*, **212**, 77 (2012).
10. B. Hu, M. Keane, M. K. Mahapatra and P. Singh, *Journal of Power Sources*, **248**, 196 (2014).
11. S. P. Jiang and Y. Zhen, *Solid State Ionics*, **179**, 1459 (2008).
12. S. P. Jiang, S. Zhang and Y. Zhen, *Journal of The Electrochemical Society*, **153**, A127 (2006).
13. D. F. Ogletree, H. Bluhm, E. D. Hebenstreit and M. Salmeron, *Nucl. Instrum. Methods Phys. Res. A*, **601**, 151 (2009).
14. A. Mitterdorfer and L. Gauckler, *Solid State Ion.*, **111**, 185 (1998).
15. J. Ralph, A. Schoeler and M. Krumpelt, *Journal of materials science*, **36**, 1161 (2001).

16. M. E. Grass, P. G. Karlsson, F. Aksoy, M. Lundqvist, B. Wannberg, B. S. Mun, Z. Hussain and Z. Liu, *Rev. Sci. Instrum.*, **81**, 053106 (2010).
17. Y. Wen, T. Yang, D. Lee, H. N. Lee, E. J. Crumlin and K. Huang, *Journal of Materials Chemistry A*, **6**, 24378 (2018).
18. E. J. Crumlin, E. Mutoro, Z. Liu, M. E. Grass, M. D. Biegalski, Y.-L. Lee, D. Morgan, H. M. Christen, H. Bluhm and Y. Shao-Horn, *Energy Environ. Sci.*, **5**, 6081 (2012).
19. M. Kubicek, G. M. Rupp, S. Huber, A. Penn, A. K. Opitz, J. Bernardi, M. Stöger-Pollach, H. Hutter and J. Fleig, *Phys. Chem. Chem. Phys.*, **16**, 2715 (2014).
20. K. A. Stoerzinger, W. T. Hong, E. J. Crumlin, H. Bluhm, M. D. Biegalski and Y. Shao-Horn, *J. Phys. Chem. C*, **118**, 19733 (2014).
21. Y. L. Yang, A. Jacobson, C. Chen, G. Luo, K. Ross and C. Chu, *Appl. Phys. Lett.*, **79**, 776 (2001).
22. Y. Yang, C. Chen, S. Chen, C. Chu and A. Jacobson, *J. Electrochem. Soc.*, **147**, 4001 (2000).
23. F. S. Baumann, J. Fleig, H.-U. Habermeier and J. Maier, *Solid State Ion.*, **177**, 1071 (2006).
24. D. Lee, R. Jacobs, Y. Jee, A. Seo, C. Sohn, A. V. Ievlev, O. S. Ovchinnikova, K. Huang, D. Morgan and H. N. Lee, *J. Phys. Chem. C*, **121**, 25651 (2017).
25. E. J. Crumlin, S.-J. Ahn, D. Lee, E. Mutoro, M. D. Biegalski, H. M. Christen and Y. Shao-Horn, *J. Electrochem. Soc.*, **159**, F219 (2012).
26. T. Yang, Y. Wen and K. Huang, in submmition.
27. J. J. Bentzen, J. V. T. Høgh, R. Barfod and A. Hagen, *Fuel Cells*, **9**, 823 (2009).
28. S. Jiang, J. Zhang and K. Foger, *Journal of The Electrochemical Society*, **147**, 3195 (2000).
29. L. Zhao, J. Drennan, C. Kong, S. Amarasinghe and S. P. Jiang, *Journal of Materials Chemistry A*, **2**, 11114 (2014).
30. X. Chen, C. Jin, L. Zhao, L. Zhang, C. Guan, L. Wang, Y.-F. Song, C.-C. Wang, J.-Q. Wang and S. P. Jiang, *international journal of hydrogen energy*, **39**, 15728 (2014).
31. E. D. Wachsman, D. Oh, E. Armstrong, D. W. Jung and C. Kan, *ECS Transactions*, **25**, 2871 (2009).
32. S. P. Simner, M. D. Anderson, G.-G. Xia, Z. Yang, L. R. Pederson and J. W. Stevenson, *Journal of The Electrochemical Society*, **152**, A740 (2005).